

Organic Bulk Heterojunction Solar Cells Based on P3HT and Anthracene-Containing PPE-PPV: Fabrication, Characterization and Modeling

SAFAE AAZOU^{a,b,c}, ASMAA IBRAL^b, MATTHEW S. WHITE^c, MARTIN KALTENBRUNNER^d, ERIC D. GŁOWACKI^c, DANIEL A. M. EGBE^c, NIYAZI SERDAR SARICIFTCI^c and EL MAHDI ASSAID^{b,*}.

^aLaboratory for Solid State Physics, Interfaces and Nanostructures, Physics Department, Liege University, Liege, Belgium.

^bLaboratory of Instrumentation, Measure and Control, Physics Department, Chouaib Doukkali University, El Jadida, Morocco.

^cLinz Institute for Organic Solar Cells (LIOS), Department of Physical Chemistry, Johannes Kepler University Linz, Altenbergerstrasse 69, A-4040 Linz, Austria.

^dDepartment of Soft Matter Physics, Johannes Kepler University, Altenbergerstrasse 69, 4040 Linz, Austria.

In this paper, a full comparative study of two different kinds of organic bulk heterojunction solar cells (OBHJ-SCs) is presented. The OBHJ-SC of the first kind is fabricated with the commonly used polymer: poly(3-hexylthiophene) (P3HT). The second one is based on a recently synthesized anthracene-containing poly(phenylene-ethynylene)-*alt*-poly(phenylene-vinylene) (PPE-PPV) bearing randomly distributed segments of octyloxy and segments of 2-ethylhexyloxy side chains and denoted **AnE-PVstat**. First, devices fabrication method is presented. Then, solar cells are characterized in dark and under AM 1.5 illumination. The incident photon conversion efficiencies (IPCE) of best cells are measured to calculate external quantum efficiencies (EQE). Next, an electronic circuit, containing photocurrent generator, non-ideal diode with its reverse saturation current and its ideality factor, series and shunt resistances, is adopted to model the fabricated solar cells. Afterwards, different methods are used to determine each solar cell model physical parameters from the current–voltage characteristics. In this way, model physical parameters extraction of **AnE-PVstat** based OBHJ-SC is done for the first time and an efficiency of around 4% is evidenced. Finally, a comparison between the performances of each kind of OBHJ-SC is achieved.

(Received April 17, 2013; accepted June 12, 2013)

Keywords: Organic bulk heterojunction solar cell, Incident photon conversion efficiency, External quantum efficiency, Model physical parameters, Parameters extraction methods

1. Introduction

In near future, it is expected that solar energy will occupy a special place among other sources of energy in the service of human beings. Indeed, humanity needs of energy are growing exponentially and conventional fossil energy resources are unable to fulfill these needs. One of the main processes for the solar energy harvesting is its conversion, via solar cells, into photovoltaic electricity. A. E. Bequerel is usually credited as being the first who demonstrated the photovoltaic effect in 1839 [1,2]. Next, a major development occurred when W. G. Adams and R. E. Day discovered, in 1876, the photoconduction effect in Selenium [3]. This led, in 1883, to the first thin film solar cell based on Selenium and fabricated by C. E. Fritts [4, 5]. The first semiconductor p–n junction solar cell was described in 1941 by Russel S. Ohl of Bell Laboratories [6, 7]. This junction was created naturally in slowly solidified melts of silicon. The study of this solar cell properties led to the understanding of the role of donor and acceptor impurities in controlling semiconductor properties and thus to the microelectronics revolution [8,

9]. For a long time, most photovoltaic solar cells produced have been based on silicon and other inorganic semiconductor p-n junctions, and were essentially made using physical techniques of growth. These kinds of solar cells can reach important efficiency and have a long lifetime [10-24]. Unfortunately, their manufacture processes are complicated and their fabrication cost is relatively expensive which slowed down solar energy development. In 1977, A. G. McDiarmid, A. J. Heeger and H. Shirakawa [25, 26] discovered electrical conductivity in chemically doped polyacetylene and laid the foundations of a discipline which will be named later organic electronics. After three decades of intensified research in the field of π -conjugated polymers aiming the development of new organic semiconductors, these eminent scientists were awarded the Nobel prize of chemistry in 2000. Since these pioneering works, enormous progress has been achieved in the design, synthesis of π -conjugated polymers and also in the fabrication, characterization and modeling of organic devices such as electroluminescent diodes based on polymers (PLEDs) [27], organic field effect transistors

(OFETs) [28] and organic photovoltaic solar cells (OPVSCs) [29]. Due to their low production cost, ease of processability, flexibility as well as tunability of their optical and electronic properties through chemical modifications, polymers present a lot of advantages in comparison to inorganic semiconductors. Their exceptional properties make them attractive candidates as advanced materials in the field of photonics and electronics [30-38]. Actually, recent development in the field of organic photovoltaic solar cells (OPVSCs) has made it possible to fabricate, according an accessible processes, low cost, lightweight and ultrathin OPVSCs on highly flexible substrates [39].

The bulk heterojunction concept which consists of intimate intermixing of donor and acceptor in the solar cell active layer has proven so far to be the best way to achieve high performance organic solar cells. In this work, we focus on two types of organic bulk heterojunction solar cells (OBHJ-SCs). For both types, (6,6)-phenyl-C61-butyric acid methyl ester (PCBM) is used as an n-type material. This molecule can take up to six electrons. The first p-type material is poly(3-hexylthiophene) (P3HT), it is a conjugated polymer and is commonly used in the fabrication of OPVSCs. The second p-type material is the recently synthesized anthracene-containing poly(*p*-phenylene-ethynylene)-*alt*-poly(*p*-phenylene-vinylene) (PPE-PPV) having statistically distributed octyloxy and 2-ethylhexyloxy side chains and denoted **AnE-PVstat** [40]. Both polymers have the same band gap of 1.9 eV but they have different chemical structures as depicted in figure 1.

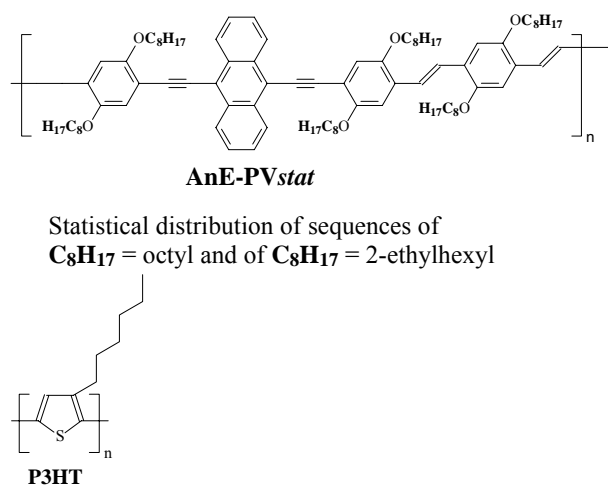


Fig. 1. Chemical structures of P3HT and AnE-PVstat.

The present paper is organized as follows: first, we present different steps of OPVSCs fabrication method from solution preparation to device construction. Then, we characterize each OPVSC in dark and under illumination, measure the incident photon conversion efficiency (IPCE) for best solar cells, and determine the external quantum efficiency (EQE). Next, we model each solar cell by an equivalent circuit containing five model physical parameters and extract all these parameters using different methods of extraction without resorting to any approximation. Finally, we achieve a full comparison of

the OPVSCs performances and show that **AnE-PVstat** based OPVSC exhibits the highest efficiency with a value $\sim 4\%$.

2. Organic bulk heterojunction solar cells fabrication

2.1. Solution preparation

The studied solar cells were prepared using two different mixtures. As we mentioned above, the p-type materials in both solutions have the same band gap but have different chemical structures (see figure 1). For the P3HT:PCBM OPVSCs, 15 mg of each component (1:1 blend) were dissolved in 1 ml chlorobenzene and 10 mg to 20 mg (1:2 blend) in 1 ml chlorobenzene. For **AnE-PVstat**:PCBM OPVSCs, the 1:1 blend solution was prepared by mixing 8 mg of each component in 1 ml chlorobenzene, while the 1:2 blend solution was obtained by dissolving 10 mg of AnE-PVstat with 20 mg of PCBM in 1 ml chlorobenzene. The prepared solutions were vigorously stirred for at least 1 hour to get a good solution.

2.2. Substrate preparation

Rigid glass indium tin oxide (glass-ITO) slides were cut into 1.5 cm width. The cut was done in one direction on the non-conductive side using diamond cutter. The ITO was cleaned from some parts to prevent short circuits (around 0.5 cm). To do so, the substrates were immersed in hydrochloric acid to etch away the ITO. To avoid etching away all the ITO, the major part of glass-ITO slide was covered with a mask, an adhesive tape that covers only the parts of glass-ITO slides where the ITO coating should remain. After etching, the substrates were rinsed with deionised water to remove the acid residue. The glass-ITO slides were then cut into 1.5 cm x 1.5 cm squares. The obtained squares were labeled in the top left corner in the non-conductive side (the side without ITO). The final cleaning process was done in an ultrasonic bath successively in special cleaning solution "hellmanex" for half an hour, in acetone for 10 minutes, in iso-propanol for 20 minutes and finally in pure water for 10 minutes.

2.3. Device fabrication

The filtered poly(3,4-ethylenedioxythiophene) : poly(styrenesulphonat) (PEDOT:PSS) was spun on each sample using the following recipe: 2000 r.p.m. for 1 second, 3000 r.p.m. for 5 seconds and 4000 r.p.m. for 25 seconds. The PEDOT:PSS is a transparent, conductive polymer with high ductility. It was used to improve the extraction properties between the ITO and the active layer and to smooth out the ITO film. The PEDOT:PSS was partly wiped away from the borders with deionized water using cotton swab. The samples were dried on a hotplate at 150 °C for 10 minutes. The prepared solution was spun at 1000 r.p.m. for 30 seconds and partly wiped away from the sample borders with toluene or chlorobenzene soaked cotton swab. The samples were then transferred to a

nitrogen-filled glovebox to dry. Finally, 100 nm Al (or 15 nm Ca and 100 nm Ag) were thermally evaporated at a pressure of 4.10^{-7} mbar (10^{-6} for the Ca|Ag contact).

2.4. Device characterisation

In the nitrogen filled glovebox, the devices were first characterized in dark and under illumination using a solar simulator (AM 1.5 global spectrum with 100 mWcm^{-2} intensity and spectral mismatch correction). A Keithley 236 source meter was used to record the current-voltage characteristics. All I-V characteristics measurements were carried out in the nitrogen filled glovebox. The incident photon conversion efficiency (IPCE) was measured for best samples to determine the external quantum efficiency (EQE). EQE is the photocurrent generated by the solar cell to the number of incoming photons at different wavelengths ratio. The device was then placed on a hotplate at 110°C for 5 to 10 minutes. After annealing, the current-voltage characteristics and the IPCE were re-measured. As reported by Egbe *et al.* [40], the devices performance enhances after annealing.

3. Organic bulk heterojunction solar cells modeling

It is well known that several non-linear electronic circuits have been used in the literature to model a solar cell. In this work, the illuminated organic bulk heterojunction solar cell (OBHJ-SC) is modeled by an electronic circuit containing five model physical parameters: a non-ideal diode with its reverse saturation current I_s and its ideality factor n , parasitic series R_s and shunt R_{sh} resistances and a photocurrent generator I_{ph} (see figure 2) [41]:

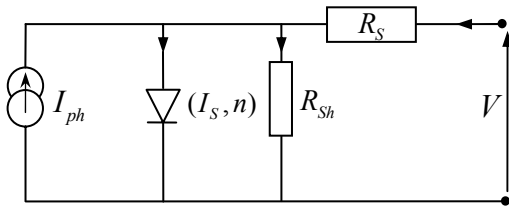


Fig. 2. Single exponential diode equivalent circuit modeling organic solar cells and including parasitic series and shunt resistances.

The solar cell characteristic equation is then given by [41]:

$$I = -I_{ph} + I_s \left(\exp\left(\frac{V - R_s I}{nV_{th}}\right) - 1 \right) + G_p(V - R_s I) \quad (1)$$

$V_{th} = k_B T/q$ is the thermal voltage, q is the electron elementary charge, k_B is the Boltzmann constant and T is the absolute temperature, $G_p = 1/R_{sh}$ is the shunt conductance. The exact analytical solution of equation (1) giving the current as a function of the voltage writes [41-43]:

$$I(V) = \frac{nV_{th}}{R_s} W \left(\frac{R_s I_s}{nV_{th}(1 + G_p R_s)} \exp\left(\frac{V + R_s(I_s + I_{ph})}{nV_{th}(1 + G_p R_s)}\right) \right) - \frac{R_s(I_s + I_{ph}) + V}{R_s(1 + G_p R_s)} + \frac{V}{R_s} \quad (2)$$

Where $W(x)$ is the multi-valued function $LambertW_k(x)$ [44]. The adequate branch for the present problem corresponds to $k = 0$ which satisfies $LambertW_0(x) = 0$ for $x = 0$.

The short-circuit current is defined as the current corresponding to $V = 0$ in equation (2):

$$I_{sc} = I(V = 0) = \frac{nV_{th}}{R_s} W \left(\frac{R_s I_s}{nV_{th}(1 + G_p R_s)} \exp\left(\frac{R_s(I_s + I_{ph})}{nV_{th}(1 + G_p R_s)}\right) \right) - \frac{I_s + I_{ph}}{1 + G_p R_s} \quad (3)$$

The output voltage analytical expression is also given as a function of $W(x)$ [42-43]:

$$V(I) = -nV_{th} W \left(\frac{I_s}{G_p nV_{th}} \exp\left(\frac{I + I_s + I_{ph}}{G_p nV_{th}}\right) \right) + \frac{I + I_s + I_{ph}}{G_p} + R_s I \quad (4)$$

The open-circuit voltage analytical expression is obtained by setting $I = 0$ in equation (4):

$$V_{oc} = V(I = 0) = -nV_{th} W \left(\frac{I_s}{G_p nV_{th}} \exp\left(\frac{I_s + I_{ph}}{G_p nV_{th}}\right) \right) + \frac{I_s + I_{ph}}{G_p} \quad (5)$$

The expressions of the output power P are :

$$P(I) = I V(I) \quad (6a)$$

$$P(V) = V I(V) \quad (6b)$$

The fill factor which is a measure of the "squareness" of the current-voltage characteristics is defined as the ratio of maximum obtainable power to the product of the open-circuit voltage and the short-circuit current:

$$FF = \frac{I_{max} V_{max}}{I_{sc} V_{oc}} \quad (7)$$

The solar cell efficiency η is the fraction of incident power ($P_{in} = 100 \text{ mW/cm}^2$) which is converted to electricity and is defined as follows:

$$\eta = \frac{FF}{P_{in}} J_{sc} V_{oc} \quad (8)$$

where J_{sc} is the short-circuit current density, which is the ratio of the short circuit current to the area of the solar cell.

4. Model physical parameters extraction methods

For a better use of OBHJ-SCs, a good knowledge of their model physical parameters is required. To that effect, solar cell current-voltage characteristics presents the most important data that should be measured, it is the bridge which allows the access to the cell optoelectronic properties. In this paper, different extraction methods are used to determine the model physical parameters appearing in the electronic circuit. These methods are based on measured current-voltage characteristics, numerical and analytical calculations of: dynamical resistance dV/dI for the first method, dynamical conductance dI/dV for the second method and the integral $\int_0^V (I - I_{sc})dV$ for the third method [41].

In all these methods and contrarily to what has been reported in the literature [41], we follow a new strategy that considers the model physical parameters themselves as variational parameters to fit the numerical data of dV/dI , dI/dV and $\int_0^V (I - I_{sc})dV$ to their respective analytical expressions. This strategy presents a lot of advantages: the numerical computations converge rapidly, the results accuracy is better and the model physical parameters are obtained directly and do not require additional calculations. Moreover, all these methods are led without any approximation or introduction of guess initial values of model physical parameters.

4.1. Dynamical resistance method

This method is based on analytical and numerical calculations of dynamical resistance $R(I, V) = dV/dI$ from the experimental $I = f(V)$ curve. The first step is the determination of the analytical expression of dV/dI from equation (4). To make this equation lighter, we write:

$$V(I) = a_1 W \left(a_2 \exp \left(\frac{I + a_3}{a_4} \right) \right) + a_5 + a_6 I \quad (9)$$

The coefficients a_i are expressed as functions of the model physical parameters:

$$a_1 = -nV_{th}, \quad a_2 = \frac{I_s}{G_p n V_{th}}, \quad a_3 = I_s + I_{ph}, \quad a_4 = G_p n V_{th},$$

$$a_5 = \frac{I_s + I_{ph}}{G_p}$$

and

$$a_6 = R_s + \frac{1}{G_p} \quad (10)$$

$$\frac{dV}{dI} = \frac{a_1 W \left(a_2 \exp \left(\frac{I + a_3}{a_4} \right) \right)}{a_4 \left(1 + W \left(a_2 \exp \left(\frac{I + a_3}{a_4} \right) \right) \right)} \quad (11)$$

The *LambertW* term contained in dV/dI is replaced using equation (9). After some algebraic calculations achieved symbolically using Maple software [45], the expression of dynamical resistance dV/dI is then given by:

$$\frac{dV}{dI} = \frac{V - a_5 - a_6 I}{\frac{a_4}{a_1} (a_1 + V - a_5 - a_6 I)} + a_6 \quad (12)$$

The last equation is rearranged symbolically using Maple software and the expression of $V dV/dI$ is determined as a function of the output current I , the output voltage V , the dynamical resistance dV/dI and the model physical parameters:

$$V \frac{dV}{dI} = R_s V - R_s (R_s + R_{sh}) I + (R_s + R_{sh}) I \frac{dV}{dI} + (nV_{th} + R_{sh} b) \frac{dV}{dI} - (nR_{sh} V_{th} + R_s (nV_{th} + R_{sh} b)) \quad (13)$$

where $b = I_s + I_{ph}$. The characteristic equation at the open-circuit point leads to the photocurrent expression:

$$I_{ph} = \frac{b + \frac{V_{oc} b}{R_{sh}}}{1 + B} \quad (14)$$

where $B = 1 / (\exp(V_{oc} / (nV_{th})) - 1)$. The saturation current is then deduced from the following equation :

$$I_s = b - I_{ph} \quad (15)$$

dV/dI and $V dV/dI$ are calculated numerically from our experimental data using Mathematica software [46]. Then a two-dimensional fitting of equation (13) to the numerical function $V dV/dI$ is carried out. Finally, the solar cell model physical parameters I_s , n , R_s , R_{sh} and I_{ph} are directly determined.

4.2. Dynamical conductance method

Many methods based on the calculation of dynamical conductance and aiming the determination of solar cell model physical parameters were reported in the literature [47-50]. In all these methods, the calculations are led with some approximations. In our case, the calculations achieved are fully analytical. The method requires the calculation of dynamical conductance $G(I, V) = \frac{dI}{dV}$ from the characteristic equation:

$$\frac{dI}{dV} = I_s \frac{1 - R_s \frac{dI}{dV}}{nV_{th}} \exp \left(\frac{V - R_s I}{nV_{th}} \right) + \frac{(1 - R_s \frac{dI}{dV})}{R_{sh}} \quad (16)$$

Starting from equation (1), we can write:

$$I_s \exp \left(\frac{V - R_s I}{nV_{th}} \right) = I + I_s + I_{ph} - \frac{(V - R_s I)}{R_{sh}} \quad (17)$$

By inserting equation (17) into equation (16) and after rearrangement, one can get an expression giving the output voltage V as a function of the output current I , the

dynamical conductance dI/dV , the model physical parameters and the output voltage V itself:

$$V = -(nV_{th}R_{sh} + bR_sR_{sh} + nV_{th}R_{sh})\frac{dI}{dV} - R_s(R_s + R_{sh})I\frac{dI}{dV} + R_sV\frac{dI}{dV} + (R_s + R_{sh})I + R_{sh}b + nV_{th} \quad (18)$$

where $b = I_s + I_{ph}$.

The photocurrent and the saturation current are calculated, as mentioned for the first method, from equations (14) and (15).

The dynamical conductance is calculated numerically from our experimental data using Mathematica software [46]. Then, a two-dimensional fitting of equation (18) to the numerical results is achieved to determine the solar cell model physical parameters I_s , n , R_s , R_{sh} and I_{ph} .

4.3. Integral method

This method is based on the analytical calculation of the Co-content function defined as [41]:

$$CC(I, V) = \int_0^V (I - I_{sc})dV \quad (19)$$

By inserting equation (2) into equation (19) and integrating with respect to V , we get an expression containing *LambertW* function and the variables V and I . The term containing *LambertW* function is then replaced using equation (2). After some algebraic calculations performed symbolically using Maple software, the Co-content function $CC(I, V)$ is expressed as :

$$CC(I, V) = \frac{G_p}{2}V^2 + \frac{R_s}{2}(1 + R_sG_p)(I - I_{sc})^2 + (nV_{th} + R_s(b + I_{sc}(1 + R_sG_p) + nG_pV_{th}))(I - I_{sc}) - (b + I_{sc}(1 + R_sG_p) + nG_pV_{th})V - R_sG_p(I - I_{sc})V \quad (20)$$

where $b = I_s + I_{ph}$.

As for the two previous methods, the photocurrent and the saturation current are calculated from equations (14) and (15).

The Co-content function is calculated numerically from our experimental data using Mathematica software. Similarly to dynamical resistance and conductance methods, a two dimensional fitting of equation (20) to the numerical results is performed to reach the solar cell model physical parameters.

5. Results and discussion

5.1. Photovoltaic metrics

Photovoltaic (PV) metrics were extracted from experimental current-voltage characteristics of different solar cells fabricated using 1:1 and 1:2 blends of P3HT:PCBM, 1:1 and 1:2 blends of **AnE-PVstat**:PCBM. They were measured before and after annealing at 110°C for 5 minutes. We remark that for solar cells based on classical polymer P3HT:PCBM, the short circuit current density J_{sc} and the open circuit voltage V_{oc} are maximum for 1:1 blend and decrease when the proportion of PCBM increases (see table 1). However, for solar cells based on **AnE-PVstat**:PCBM, the short circuit current density J_{sc} and the open circuit voltage V_{oc} are greater for 1:2 blend than for 1:1 blend (see table 1).

Table 1: Experimental photovoltaic metrics from solar cells made with different blend ratios of P3HT:PCBM and AnE-PVstat:PCBM, and measured after annealing at 110 °C for 5 minutes. Best metrics for each ratio are underlined.

	1:1 Blends		1:2 Blends	
	P3HT:PCBM 15 mg:15 mg	AnE- PVstat:PCBM 8 mg:8 mg	P3HT:PCBM 10 mg:20 mg	AnE- PVstat:PCBM 10 mg:20 mg
J_{sc} (mA/cm ²)	<u>10.8</u>	4.75	5.50	<u>9.12</u>
V_{oc} (mV)	572.7	<u>774.5</u>	548	<u>822.3</u>
I_m (mA)	<u>0.67</u>	0.31	0.39	<u>0.69</u>
V_m (mV)	373.4	<u>540</u>	353	<u>600</u>
FF %	<u>46</u>	45	45	<u>56</u>
η %	<u>2.87</u>	1.41	1.25	<u>4.17</u>

To understand these results, we emphasize that in organic donor-acceptor solar cells, light is mostly absorbed in donor material, which corresponds in our case to P3HT or **AnE-PVstat**. The absorption of one photon leads to the

generation of an interacting electron-hole pair called singlet exciton (X) in donor material. Due to low dielectric screening in organic semiconductors ($\epsilon_r(\text{P3HT}) = 3$ [52], $\epsilon_r(\text{PCBM}) = 3.9$ [53]), the correlated electron-hole (X)

binding energy is larger in comparison to binding energy in inorganic semiconductors. After photogeneration, the electron-hole pair (X) diffuses to distributed junction between n-type and p-type materials where transitions of holes to highest occupied molecular orbital (HOMO) and electrons to lowest unoccupied molecular orbital (LUMO) of the donor material occur. Then hole flees to the anode and electron hops to LUMO of the acceptor material and runs away to the cathode. In summary, the macromolecule ensures light absorption and holes conduction and the

small molecule guarantees the electrons conduction by hopping from one localized state to the next. When the proportion of donor material increases, light absorption increases and electron mobility decreases. When the proportion of acceptor material increases, electron mobility increases and light absorption decreases. For P3HT:PCBM solar cells, optimum photovoltaic properties are obtained with 1:1 blend (see tables 1 and 2). For **AnE-PVstat**:PCBM solar cells, best photovoltaic qualities are attained with 1:2 blend (see tables 1 and 2).

Table 2: Model physical parameters and calculated photovoltaic metrics of solar cells made with 1:1 and 1:2 blend ratios of P3HT:PCBM and AnE-PVstat:PCBM. The model physical parameters are obtained via dynamical conduction extraction method. The most efficient cell is that made with 1:2 blend of AnE-PVstat:PCBM which presents highest values of FF and η . Absolute optimal values are underlined.

	P3HT:PCBM		AnE – PVstat:PCBM	
	1:1 (15mg: 15mg)	1:2 (10mg: 20mg)	1:1 (8mg: 8mg)	1:2 (10mg: 20mg)
$R_s(\Omega)$	64.36	386.92	<u>38.025</u>	46.21
$R_{sh}(k\Omega)$	3.364	3.01	3.842	<u>5.96</u>
$I_s(nA)$	<u>$4.94 \cdot 10^3$</u>	$5.73 \cdot 10^{-8}$	7.09	16.57
n	4.23	<u>0.71</u>	2.84	2.97
$I_{ph}(mA)$	<u>1.08</u>	0.615	0.471	0.893
$J_{sc}(mA/cm^2)$	<u>10.56</u>	5.45	4.67	8.86
$V_{oc}(mV)$	571.7	548	774.5	<u>822.3</u>
$I_m(mA)$	<u>0.741</u>	0.412	0.299	0.70
$V_m(mV)$	368.2	331	572.3	<u>617.2</u>
FF(%)	45	47	47	<u>59</u>
η (%)	2.73	1.41	1.45	<u>4.3</u>

5.2. Model physical parameters extraction

It is important to underline that knowledge of device model physical parameters is an essential tool for a good understanding of transport mechanisms and optical processes involved in an optoelectronic device [54]. Series resistance is due to: i) voltage drop across PEDOT:PSS and active layer of OBHJ-SC, ii) contact resistance between metal and organic semiconductor, iii) contact resistance between transparent conductive oxide (ITO) and PEDOT:PSS, iv) sheet resistances of the front and back metal contacts. Parallel or shunt resistance arises from leakage of current through the cell, around edges of the device and between contacts of different polarity. Saturation current is a sum of one term proportional to the number of electrons in LUMO of n-type material and a second term proportional to the number of holes in HOMO of p-type material in dark conditions, it expresses i) the aptitude of some singlet excitons to be dissociated due to thermal agitation, ii) the ability of electron to move along the acceptor small molecule by jumping from one localized state to the next or by hopping from one small molecule to the next, ii) the ability of hole to move along

the donor macromolecule. Ideality factor tells about recombination transition mechanisms that occur in the distributed junction: $n \approx 1$ means that recombination processes are negligible, $n \approx 2$ corresponds to band-to-band (HOMO-to-LUMO) recombination; $n > 2$ indicates that more complex recombination processes such as extrinsic Shockley-Read-Hall or Auger generation-recombination processes occur. Finally, photocurrent is proportional to the number of photons absorbed and converted to uncorrelated electron-hole pairs.

Experimental $J-V$ data were measured according characterization process reported in section 2. Linear-linear and log-linear $J-V$ characteristics in dark and under one sun illumination were depicted in figures 3, 4, 5 and 6 respectively for P3HT:PCBM 1:1 blend, 1:2 blend, **AnE-PVstat**:PCBM 1:1 blend and 1:2 blend. Experimental $J-V$ data were also used by means of the methods described in section 4 to extract all prepared solar cells model physical parameters. A comparative study of deviations between optimized and experimental curves shows that dynamical conductance extraction method leads to the closest curves to experimental data (see figures 3 to 6).

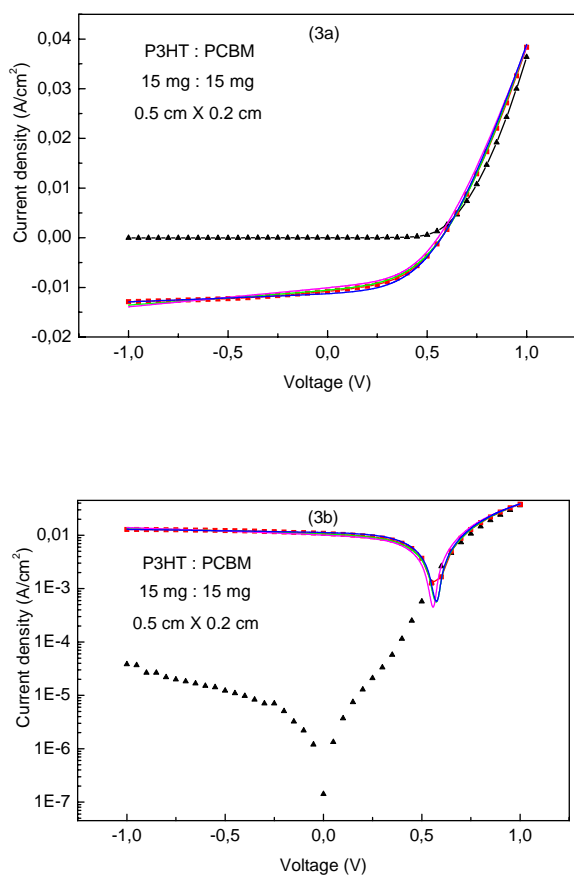


Fig. 3. Linear-linear (3a) and log-linear (3b) J - V characteristics of 0.1 cm^2 solar cell fabricated using 1:1 blend of P3HT:PCBM and a Ca(15nm)|Ag(100nm) metal contact. Black triangles correspond to dark characteristics, red squares correspond to one sun illuminated solar cell characteristics. This device has $\sim 3\%$ efficiency which is the best result reached with P3HT based solar cells. The optimized characteristics are obtained using the presented methods. The magenta, blue and green lines correspond respectively to integral, dynamical resistance and dynamical conductance methods.

The log-linear J - V curves of 1:1 P3HT:PCBM and 1:2 **AnE-PVstat**:PCBM blends show that in dark conditions, these solar cells show a rectification ratio of approximately 10^3 . This is an indication of efficient polarization of the device in the forward bias where electrons are injected from a low work function electrode (Al for **AnE-PVstat**, and Ca|Ag for P3HT) to the LUMO of the blend while holes are injected from a high work function electrode to the HOMO of the blend. It is an evidence of a good forward biased diode [40, 55].

The thicknesses of ITO and PEDOT:PSS layers are respectively equal to 150 nm and 40 nm [56]. So, the resistances of ITO, PEDOT:PSS, Al and Ca|Ag do not exceed a few ohms for each sheet ($\sum_i R_i < 10 \Omega$). We can hence state that for a fixed p-type to n-type ratio (1:1 or 1:2), cells based on **AnE-PVstat** always exhibit small series resistance and high shunt resistance in comparison to cells based on conventional polymer (see table2) which means that voltage drop across the active layer is higher and the injection resistance between PEDOT:PSS and active layer and contact resistance between metal and organic semiconductor in former cells are lower.

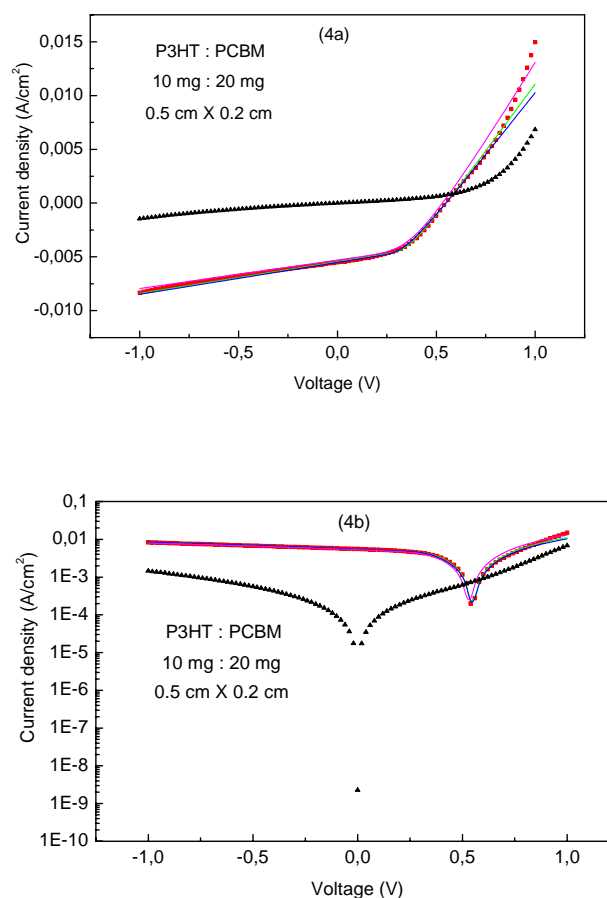


Fig. 4. Linear-linear (4a) and log-linear (4b) J - V characteristics of 0.1 cm^2 solar cell made using 1:2 blend of P3HT:PCBM and an Al(100nm) metal contact. Black triangles correspond to dark characteristics, red squares correspond to one sun illumination. This device has $\sim 1.25\%$ efficiency. The optimized characteristics are obtained using the extraction methods. The magenta, blue and green lines correspond respectively to integral, dynamical resistance and dynamical conductance methods.

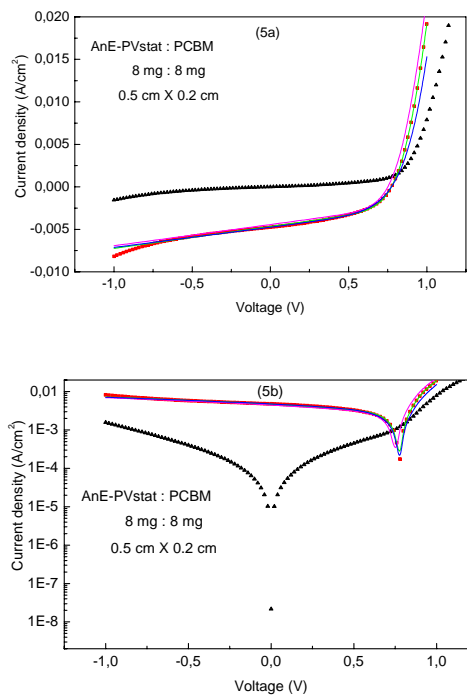


Fig. 5. Linear-linear (5a) and log-linear (5b) J - V characteristics of 0.1 cm^2 organic solar cell fabricated using 1:1 mixture of AnE-PVstat:PCBM and an Al(100nm) metal contact. Black triangles correspond to dark characteristics and red squares to one sun illumination. This device has $\sim 1.4\%$ efficiency.

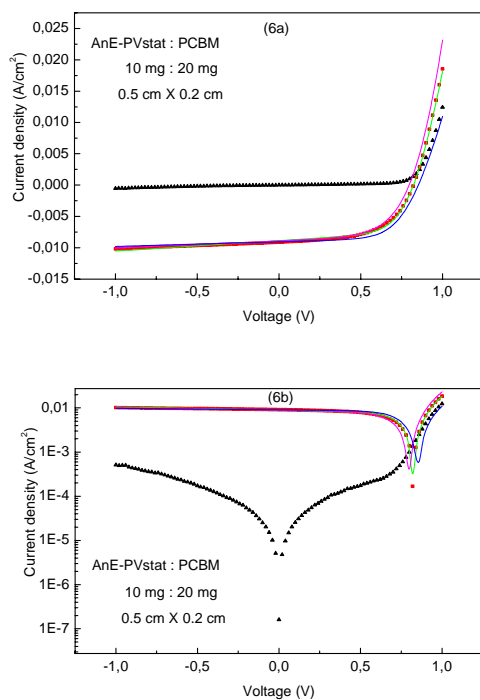


Fig. 6. Linear-linear (6a) and log-linear (6b) J - V characteristics of 0.1 cm^2 solar cell made using 1:2 blend of AnE-PVstat:PCBM and an Al(100nm) metal contact. Black triangles correspond to dark characteristics and red squares to one sun illumination. This cell presents an efficiency of $\sim 4\%$.

5.3. External quantum efficiency measurements

In Fig. 7, EQE of best solar cells made with 1:1 blend ratio of P3HT:PCBM (red line), and 1:2 blend ratio of AnE-PVstat:PCBM (green line) are plotted against the incident photon wavelength. For the second polymer, one can remark a collection of energy states just above the bandgap, ranging from green to red and corresponding to the right peak and another collection of slightly higher energy states ranging from 340 nm to 460 nm corresponding to the left peak. The two peaks overlap a little bit in the middle in the blue absorption zone around 472 nm where the EQE of the first polymer is larger than that of the second polymer (the region from 424 nm to 560 nm). This zone coincides with the region around the maximum of the solar radiation spectrum. This means that P3HT absorbs more than AnE-PVstat which suggests that higher efficiency measured in the case of the second polymer (see table 1) is rather due to improved charge carrier mobilities than to higher absorption.

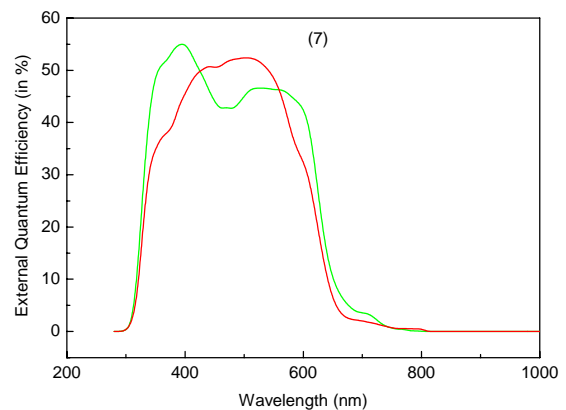


Fig. 7. EQE curves of the best solar cells made using 1:2 blend of AnE-PVstat:PCBM (green line) and 1:1 blend of P3HT:PCBM (red line).

5.4. Comparison of the blends 1:1 P3HT:PCBM and 1:2 AnE-PVstat:PCBM

With regards to what has been seen above, the question that may arise is: what is the appropriate blend that could allow the fabrication of organic solar cells with optimum qualities? Answer to such question is somewhat difficult since each blend has its own advantages. Indeed, in view of what has been seen in section 5 and taking into consideration the model physical parameters summarized in table 2, we can state that solar cells based on 1:1 P3HT:PCBM blend presents the highest values of saturation current, photogeneration current, short-circuit current and maximum power point current. These assets are due to enhanced absorption of this mixture in 424 nm to 560 nm zone. Nevertheless, solar cells based on 1:2 AnE-PVstat:PCBM blend exhibits small series resistance, highest values of shunt resistance, open-circuit voltage and maximum power point voltage. These qualities are due to improved charge carrier mobilities [40], which is mainly

due to the presence of triple bonds on both sides of the anthracene (see Fig. 1).

6. Conclusion

We performed a comparative study of electrical characteristics and efficiencies of solar cells fabricated using two different polymers: the common P3HT and **AnE-PVstat** which is a side chain based statistical copolymer resulting from random distribution of segments of linear octyloxy side chains and of branched 2-ethylhexyloxy side chains, on the backbone of anthracene containing poly(*p*-phenylene-ethynylene)-*alt*-poly(*p*-phenylene-vinylene) (PPE-PPV). An efficiency of ~4% has been achieved for solar cells based on 1:2 **AnE-PVstat**:PCBM blend. Organic solar cells were fabricated using four different blends : 1:1 and 1:2 ratios of P3HT:PCBM blend, 1:1 and 1:2 ratios of **AnE-PVstat**:PCBM blend. Then they were characterized in dark and under one sun illuminated conditions. A five model physical parameters electronic circuit was used to model each organic solar cell. Three different methods for model physical parameters extraction were presented. These methods fit the exact analytical expression of dynamical conductance, dynamical resistance and area under the current-voltage characteristics respectively to numerical values of dI/dV , dV/dI and $\int_0^V (I - I_{sc})dV$, which were calculated from $I - V$ curve, according to a new strategy that used model physical parameters as variational parameters to minimize error between experimental and optimized data. This strategy led directly to model physical parameters and gave closest optimized curves to experimental current-voltage characteristics. Organic solar cells photovoltaic metrics showed that the blend ratios presenting the best performance are 1:1 for P3HT:PCBM and 1:2 for **AnE-PVstat**.

Acknowledgments

Safae AAZOU is grateful to CNRST of Morocco for its financial support under grant N° E12/001. She is also thankful to ERASMUS MUNDUS fund for its financial assistance and to the African Network for Solar Energy (ANSOLE) for enabling her to carry out studies at LIOS (Austria) in the framework of ANSOLE ANEX program. Daniel A. M. Egbe acknowledges the financial support of the Deutsche Forschungsgemeinschaft (DFG) in the framework of the priority program SPP1355.

References

- [1] A. E. Becquerel, C. R. Acad. Sci. **9**, 145 (1839).
- [2] A. E. Becquerel, C. R. Acad. Sci. **9**, 561 (1839).
- [3] W. G. Adams, R.E. Day, Proc. Roy. Soc. London A **25**, 113 (1877).
- [4] C. E. Fritts, Proc. Am. Assoc. Adv. Sci. **33**, 97 (1883).
- [5] C. E. Fritts, Am. J. Sci. **26**, 465 (1883).
- [6] R.S. Ohl, Light-sensitive electric device, US Patent No. 2, 402, 622, 27th May 1941.
- [7] R.S. Ohl, Light-sensitive device including silicon, US Patent No. 2,443,542, 27th May, 1941.
- [8] M. A. Green, Photovoltaics: coming of age, Conference on Record, 21st IEEE Photovoltaic Specialists Conference, Kissimmee, May 1990, p. 1.
- [9] M. Riordan, L. Hoddeson, Crystal Fire, Norton, New York (1997).
- [10] T. Dullweber, G. Hanna, U. Rau, H.W. Schock, Solar Energy Materials & Solar Cells **67**, 145 (2001).
- [11] M.A. Green, J. Zhao, A. Wang, S.R. Wenham, Progress and outlook for high-efficiency crystalline silicon solar cells, Solar Energy Materials & Solar Cells **65**, 9-16 (2001).
- [12] H. E. A. Elgamel, J. Gobrecht, Solar Energy Materials & Solar Cells **65**, 561 (2001).
- [13] K. Nakajima, N. Usami, K. Fujiwara, Y. Murakami, T. Ujihara, G. Sasaki, T. Shishido, Solar Energy Materials & Solar Cells **73**, 305-320 (2002).
- [14] J. Zhao, Solar Energy Materials & Solar Cells **82**, 53 (2004).
- [15] M. Yamaguchia, T. Takamoto, K. Arakia, Solar Energy Materials & Solar Cells **90**, 3068 (2006).
- [16] S.W. Glunz, Solar Energy Materials & Solar Cells **90**, 3276 (2006).
- [17] M. Yamaguchi, K. Nishimura, T. Sasaki, H. Suzuki, K. Arafune, N. Kojima, Y. Ohsita, Y. Okada, A. Yamamoto, T. Takamoto, K. Araki, Solar Energy **82**, 173 (2008).
- [18] J. Lee, N. Lakshminarayan, S. K. Dhungel, K. Kim J. Yi, Solar Energy Materials & Solar Cells **93**, 256 (2009).
- [19] Y. Tsunomura, Y. Yoshimine, M. Taguchi, T. Baba, T. Kinoshita, H. Kanno, H. Sakata, E. Maruyama, M. Tanaka, Solar Energy Materials & Solar Cells **93**, 670 (2009).
- [20] D.J. Friedman, Current Opinion in Solid State and Materials Science **14**, 131 (2010).
- [21] N. Auriac, B. Grange, R. Cabal, A. Maris-Froelicha, P.J Ribeyron, Energy Procedia **8**, 427 (2011).
- [22] T. Mishima, M. Taguchi, H. Sakata, E. Maruyama, Solar Energy Materials & Solar Cells **95**, 18 (2011).
- [23] X. Gu, X. Yu, K. Guo, L. Chen, D. Wang, D. Yang, Solar Energy Materials & Solar Cells **101**, 95 (2012).
- [24] A. Chen, Z. Kaigui, Solar Energy **86**, 393 (2012).
- [25] C. K. Chiang, C. R. Fischer, Y. W. Park, A. J. Heeger, H. Shirakawa, E. J. Louis, S. C. Gau, A. G. MacDiarmid, Phys. Rev. Lett. **39**, 1098 (1977).
- [26] C. K. Chiang, M. A. Druy, S. C. Gau, A. J. Heeger, E. J. Louis, A. G. MacDiarmid, Y. W. Park, H. Shirakawa, J. Am. Chem. Soc. **100**, 1013 (1978).
- [27] S. T. Kim, D. H. Hwang, X. C. Li, J. Grüner, R. H. Friend, A. B. Holmes, H. K. Shim, Advanced Materials **8**, 979 (1996).

- [28] L. L. Chua, J. Zaumseil, J. -F. Chang, E. C. -W. Ou, P. K. H. Ho, H. Sirringhaus, R. H. Friend, *Nature* **434**, 194 (2005).
- [29] S. Günes, H. Neugebauer, N. S. Sariciftci, *Chem. Rev.* **107**, 1324 (2007).
- [30] S. R. Forrest, *Nature* **428**, 911 (2004).
- [31] H. Klauk, *Organic Electronics*, Wiley-VCH, Weinheim, New York (2006).
- [32] H. Shirakawa, E. J. Louis, A. G. MacDiarmid, C. K. Chiang, A. J. Heeger, *J. C. S. Chem. Comm.*, 578-580 (1977).
- [33] Z. Bao, J. Locklin, *Organic Field Effect Transistors*, Taylor and Francis, Boca Raton, FL (2007).
- [34] S. S. Sun, L. Dalton, *Introduction to Organic Electronic and Optoelectronic Materials and Devices*, Taylor & Francis, Boca Raton, FL (2008).
- [35] A. Moliton, *Optoelectronics of Molecules and Polymers*, Springer-Verlag, Berlin, Germany (2006).
- [36] G. Hadziioannou and G. G. Mallarias, *Semiconducting Polymers*, Wiley-VCH, Weinheim, Germany (2007).
- [37] R. Shinar, J. Shinar, *Organic Electronics in Sensors and Biotechnology*, McGraw-Hill, New York (2009).
- [38] H. S. Nalwa, *Handbook of Organic Electronics and Photonics*, American Scientific Publishers, Valencia, CA (2008).
- [39] M. Kaltenbrunner, M. S. White, E. D. Glowacki, T. Sekitani, T. Someya, N. S. Sariciftci, S. Bauer, *Nature Communications* **3**, 1-7 (2012). DOI: 10.1038/ncomms1772.
- [40] D. A. M. Egbe, G. Adam, A. Pivrikas, A. M. Ramil, E. Birckner, V. Cimrova, H. Hoppe, N. S. Sariciftci, *Journal of Materials Chemistry* **20**, 9726 (2010).
- [41] A. Ortiz-Conde, F. J. Garcia Sanchez, J. Muci, *Solar Energy Materials and Solar Cells* **90**, 352 (2006).
- [42] A. Jain, A. Kapoor, *Solar Energy Materials and Solar Cells* **81**, 269 (2004).
- [43] S. Aazou, E. Assaid, Modelling real photovoltaic solar cell using Maple, 21st IEEE International Conference on Microelectronics, Marrakesh, December, 2009, p. 394-397.
- [44] R. M. Corless, G. H. Gonnet, D. E. G. Hare, D. J. Jeffrey, D. E. Knuth, *Advances in Computational Mathematics* **5**, 329 (1996).
- [45] Maple V Release 15, Copyright 1981-2012, Waterloo Maple Inc.
- [46] Mathematica 8, Copyright 1988-2010, Wolfram research Inc.
- [47] Z. Ouennoughi, M. Chegaar, *Solid-State Electronics* **43**, 1985 (1999).
- [48] M. Chegaar, Z. Ouennoughi, A. Hoffmann, *Solid-State Electronics* **45**, 293 (2001).
- [49] M. Chegaar, Z. Ouennoughi, F. Guechib, *Vacuum* **75**, 367 (2004).
- [50] K. Bouzidi, M. Chegaar, M. Aillerie, *Energy Procedia* **18**, 1601 (2012).
- [51] C. Deibel, V. Dyakonov, *Rep. Prog. Phys.* **73**, 96401 (2010).
- [52] J. W. Jung, W. H. Jo, *Adv. Funct. Mater.* **20**, 1 (2010).
- [53] H. Hoppe, N. S. Sariciftci, D. Meissner, *Mol. Cryst. Liq. Cryst.* **385**, 113 (2002).
- [54] Stephen J. Fonash, *Solar Cell Device Physics*, Second Edition, Academic Press, Amsterdam (2010).
- [55] G. Yu, A. J. Heeger, *J. Appl. Phys.* **78**, 4510 (1995).
- [56] S. Kraner, Measurement of charge carrier mobility and charge carrier concentration of organic photovoltaic diodes under in situ light soaking conditions and varying temperatures, Master of Sciences Thesis, Johannes Kepler University Linz, Austria (2011).

*Corresponding author: eassaid@yahoo.fr